Critical properties of highly frustrated pyrochlore antiferromagnets

J. N. Reimers,* J. E. Greedan, and M. Björgvinsson

Institute for Materials Research, McMaster University, Hamilton, Ontario, Canada L8S 4M1

(Received 15 August 1991)

The pyrochlore form of FeF_3 (pyr-FeF_3) exhibits an unusual noncoplanar form of long-range magnetic order below 16 K. This is a result of the topological frustration inherent in the lattice of corner-sharing tetrahedra formed by the iron atoms. Neutron-diffraction experiments fix the critical exponent β at 0.18(2), which does not correspond to any known universality class. Monte Carlo simulations on the same lattice with Heisenberg spins confirm this value of β and also determine that $\nu=0.38(2)$, $\gamma=1.1(1)$, and $\alpha=0.6(1)$. The power of Ferrenberg and Swendsen's histogram method of Monte Carlo data analysis is discussed, as well as careful checks for weak first-order behavior in the transition. The recently discovered universality classes in triangular-lattice antiferromagnets are compared to the situation in pyr-FeF_3.

I. INTRODUCTION

Frustration in magnetic systems is well known to be responsible for a number of diverse phenomena such as spin-glass behavior,[1] noncollinear and incommensurate order,[2] and unusual critical properties.[3] Recently there has been much interest and controversy over the critical properties in frustrated triangular antiferromagnets. With vectors spins (XY or Heisenberg) these systems will order with three magnetic sublattices forming 120° angles with nearest neighbors on the other sublattices.

Kawamura has pointed out using Monte Carlo simulations that triangular-lattice antiferromagnets (TLAF's) exhibit unusual critical exponents.[3,4] In particular, the exponents for TLAF's with XY spins [$\beta=0.253(10)$, $\gamma=1.13(5)$, $\nu=0.54(2)$, $\alpha=0.34(6)$] (Ref. 3) and Heisenberg spins [$\beta=0.30(15)$, $\gamma=1.17(7)$, $\nu=0.59(2)$, $\alpha=0.25(5)$] (Ref. 4) are in no way similar to the standard $O(n)$ critical exponents where $n=2$ for XY ($\beta=0.345$, $\gamma=1.316$, $\nu=0.669$, $\alpha=-0.01$) (Ref. 5) and $n=3$ for Heisenberg ($\beta=0.367$, $\gamma=1.388$, $\nu=0.707$, $\alpha=-0.121$).[5] Thus, TLAF's with vector spins belong to different universality classes. This is a counterexample to the popular misconception that universality classes can be characterized by the spin dimensionality. As originally stated by Griffiths,[6] one must consider the symmetry of the order parameter (which reduces to spin dimensionality only in simple cases) when characterizing universality classes. This idea can be understood by realizing that the symmetry of the order parameter determines the form of the Ginzberg-Landau-Wilson (GLW) Hamiltonian, which, in turn, governs the critical properties upon renormalization. In fact, Kawamura has suggested that both the $\varepsilon=4-d$ and $1/n$ expansion treatments of TLAF's exhibit a fixed point not present for $O(n)$ systems.[7] These critical exponents have been confirmed by neutron-scattering experiments on $CsMnBr_3$,[8] Holmuim,[9] and VCl_2,[10] and most recently by careful heat-capacity measurements on $CsMnBr_3$.[11]

The unusual exponents are also a source of controversy for three reasons.

(1) The critical point in $CsMnBr_3$ has been shown to be a *tetra*critical point and multicritical points are well known to exhibit unusual critical properties. However, such multicritical behavior is consistent with the occurrence of a different universality class.[12]

(2) These exponents are not far, numerically, from the mean-field tricritical exponents ($\beta=0.25$, $\gamma=1$, $\nu=0.5$, and $\alpha=0.5$). Azaria et al.[13] have proposed such an interpretation based on their renormalization-group calculations ($d=2+\varepsilon$).

(3) Reluctance to part with the simple idea that universality classes are governed by spin dimensionality.

These interesting results have stimulated an investigation of critical properties in pyrochlores. In the pyrochlore form of FeF_3 (referred to as pyr-FeF_3), the metal atoms form an infinite three-dimensional lattice of corner-sharing tetrahedra. Antiferromagnetic ordering on such a lattice is highly frustrated. This can be partially understood by realizing that no spin configuration exists which simultaneously satisfies all six antiferromagnetic interactions on a single tetrahedron. This same difficulty is also present on the fcc lattice, which can be thought of as a lattice of *edge*-sharing tetrahedra. Antiferromagnetic ordering in pyrochlores is further inhibited because the tetrahedra are *corner* sharing and thus more sparsely connected than in the fcc counterpart.

pyr-FeF_3 was synthesized by De Pape et al.,[14] with cell edge $a=10.324(2)$ Å and cubic space group $Fd\bar{3}m$. Subsequently, Ferey et al.[15] determined the magnetic structure below 16 K, which consists of four sublattices (corresponding to the four corners on a tetrahedron) oriented along the four cubic (111) directions (see Fig. 1). This noncoplanar order seems to be, in some sense, a three-dimensional analog of the coplanar (but noncollinear) ordering observed in the TLAF's.

The objective of this work is to investigate the critical properties of pyrochlore antiferromagnets. First, experimentally in pyr-FeF_3 and secondly, through extensive Monte Carlo (MC) simulations with finite-size scaling.
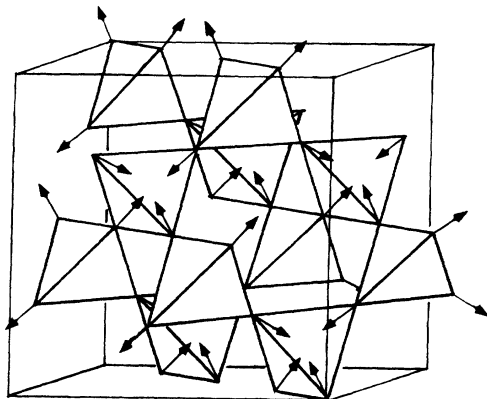
FIG. 1. The three-dimensional network of corner-sharing tetrahedra formed by one of the metal sublattices in pyrochlores. An outline of the cubic unit cell is also shown. Arrows are a schematic representation of the noncoplanar magnetic structure in pyr-FeF$_3$.

The experimental and MC results both strongly suggest that the pyrochlore antiferromagnet belongs to a universality class characterized by an order-parameter space isomorphic to $S_2 \times \mathbb{Z}_3$. In Sec. II we describe the results of neutron-diffraction experiments on pyr-FeF$_3$. A brief review of mean-field-theory results which suggest a suitable exchange model for the simulations is outlined in Sec. III. Section IV contains some technical details of the Monte Carlo methods employed and the results for the elementary thermodynamic functions. Section V is an extensive discussion of methods for determining the order of a phase transition with MC data and a respective application of these methods to our data. Critical exponents for the transition are determined using finite-size scaling analysis in Sec. VI and Sec. VII contains a discussion of collinearity of the ordered state in the MC simulations. A summary and concluding remarks can be found in Sec. VIII.

II. CRITICAL PROPERTIES IN pyr-FeF$_3$

In order to determine the critical exponent β, we have carried out neutron-diffraction experiments on a powder sample of pyr-FeF$_3$. The sample was prepared following the procedure outlined in Ref. 14. Great care was taken in removing residual ammonia from the sample in order to minimize the incoherent scattering due to hydrogen. The measurements were carried out at the McMaster Nuclear Reactor using 1.39 Å neutrons and a position-sensitive detector. For the determination of β, data in the range of $1.16 \leq Q \leq 2.94$ Å were considered, which contain scattering from the first four magnetic Bragg reflections. Twelve data sets were collected from 7.5 to 15.5 K and analyzed with Rietveld profile fitting in order to determine an ordered moment at each temperature.

A magnetic moment of $[3.36(3)]\mu_B$ was observed at 7.5 K, which is in agreement with Ferey's result[15] but lower than the theoretical value which is naively expected to be near $5\mu_B$. Such low magnetic moments have also been observed in many of the triangular antiferromagnets

where the effect is believed to be caused by quantum spin fluctuations.[16] For temperatures closest to T_c, it was necessary to account for a small amount of critical scattering near the Bragg peaks. This was modeled with a resolution convoluted Lorentzian. Since the intensity of the critical scattering is statistically correlated with the Bragg peak intensities, the estimated errors in the refined magnetic moments increase near T_c. The refinement was, however, constrained in that all four magnetic Bragg peaks had the same fraction of critical scattering with the same correlation length, and the Gaussian Bragg peak widths were set equal to the nuclear peak widths.

The measured magnetic moments were fitted using a power law of the form

$$\mu(T) \propto t^\beta , \tag{1}$$

where

$$t = (T_c - T)/T_c \tag{2}$$

is the reduced temperature. The best fit to (1) is shown in Fig. 2 giving $\beta = 0.18(2)$ and $T_c = 15.4(1)$ K, using a reduced temperature range of $0.01 \leq t \leq 0.3$. As is always the case, β is somewhat dependent on the choice of T_c. In this case when T_c was varied by ± 0.1 K, χ^2 for the fit roughly doubled and β changed by approximately ± 0.02, thus defining the e.s.d.'s (estimated standard deviations) in β and T_c. The datum at 7.5 K was excluded from the analysis.

The value obtained for β is vastly different from any of the exponents for the O(n) models which range from 0.326 [O(1)=Ising] to 0.367 [O(3)=Heisenberg].[5] In light of the unusual exponents in frustrated TLAF's, where β ranges from 0.25 (Ref. 3) to 0.30,[4] the low exponent observed in pyr-FeF$_3$ does not come as a complete surprise. The presence of critical scattering provides evidence that the transition is most likely second order. Measurements of other exponents γ and ν with neutrons are also possible, in principle, but, in practice, this is not viable without a large single crystal. However, a measurement of α in the heat capacity should be possible. This has been attempted[17] without satisfactory results.
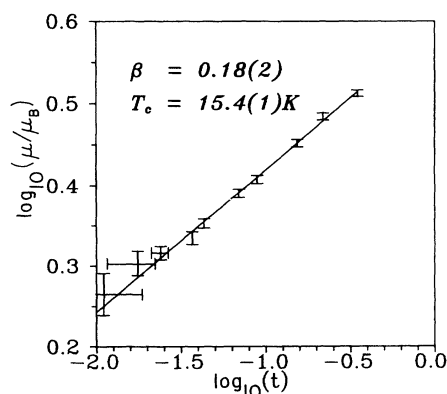

FIG. 2. log-log plot of the measured magnetic moment in pyr-FeF$_3$ vs reduced temperature, $t = (T_c - T)/T_c$, giving $\beta = 0.18(2)$ and $T_c = 15.4(1)$ K.

The heat-capacity peak was rounded considerably by particle size or surface area effects. A similar problem has occurred in dysprosium aluminum garnet[18] where heat-capacity data were observed to be much more sensitive to particle size effects than the neutron-diffraction data. At the moment, the only way to make further progress on this interesting phase transition is to simulate the system using a reasonable exchange model. In the next section we will describe and justify such a model.

III. MEAN-FIELD THEORY

A detailed analysis of magnetic ordering in pyrochlores can be found in Ref. 19. Therein a general Landau theory calculation is carried out in which no *a priori* assumptions are made about the nature of the highest-temperature ordered phase. In other words, all Fourier modes were considered and a variety of exchange models were analyzed, including interactions out to fourth neighbors.

As stated previously, the metal atoms in pyr-FeF$_3$ lie on the 16c site in the space group $Fd3m$ and form a three-dimensional lattice of corner-sharing tetrahedra. Because of the face centering, it is possible to choose a primitive rhombohedral unit cell which has only one-quarter the volume of the cubic unit cell, thereby reducing the number of magnetic atoms per cell from 16 to 4 and simplifying any algebraic work considerably. The mean-field results will be discussed in terms of the primitive unit cell. Because there are four magnetic atoms per primitive cell, there will be four normal modes for every q (wave vector) in the zone. For the simplest model, in which the nearest-neighbor interaction J_1 is less than zero (antiferromagnetic) and further-neighbor interactions are zero, no long-range order is predicted within the mean-field approximation. At the mean field T_c, $2N$ out of the $4N$ (N is the number of primitive unit cells) become critical (χ_q diverges). Thus, the system preferentially selects a phase space with half the dimensionality below T_c. This reduced phase space is not sufficiently restrictive to stabilize long-range order. Monte Carlo simulations of this model have shown that no long-range order occurs at any temperature.[20] In fact, the majority of pyrochlore antiferromagnets studied to date show no long-range magnetic order but instead exhibit spin-glass-like behavior.[21]

In some cases, long-range order is stabilized when further-neighbor interactions are included. Figure 3 shows a phase diagram in the space of J_2 and J_3, the second- and third-neighbor exchange constants. Different regions in the phase diagram are characterized by the wave vector of the highest-temperature ordered phase. The diagram is dominated by regions of incommensurate order. The dotted line for $J_3 < 0$ indicates that there is a degeneration line in q space and therefore no long-range order within mean-field theory. Of interest for this work is the region on the right of the phase diagram ($J_3 > 0$) where the q=0 phase is stable. This corresponds to the situation in pyr-FeF$_3$. In this case there are three degenerate normal modes that go critical
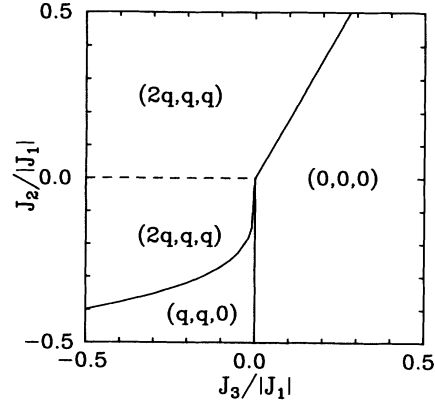

FIG. 3. Phase diagram of ordering wave vectors in the exchange constant space of J_2 and J_3, as determined by mean-field theory (from Ref. 19). The dashed line for $J_3 < 0$ indicates that the system has a degeneration line in q space and no long-range order is predicted. On the right half ($J_3 > 0$) of the diagram, phases with q=0 are stable, which is relevant to pyr-FeF$_3$.

$$\varphi_1 = \tfrac{1}{2}(\mathbf{m}_1 + \mathbf{m}_2 - \mathbf{m}_3 - \mathbf{m}_4) ,$$

$$\varphi_2 = \tfrac{1}{2}(\mathbf{m}_1 - \mathbf{m}_2 + \mathbf{m}_3 - \mathbf{m}_4) , \qquad (3)$$

$$\varphi_3 = \tfrac{1}{2}(\mathbf{m}_1 - \mathbf{m}_2 - \mathbf{m}_3 + \mathbf{m}_4) ,$$

where $\mathbf{m}_a$ is the net magnetization on sublattice a. Within mean-field theory these modes can mix in any way subject to an orthogonality constraint

$$\varphi_1 \cdot \varphi_2 = \varphi_2 \cdot \varphi_3 = \varphi_3 \cdot \varphi_1 = 0 \qquad (4)$$

imposed by higher-order terms in the Landau expansion. The implications of this will be discussed further in Sec. VII. It is also worth pointing out that mean-field theory predicts that the phase transition is continuous. However, mean-field theory is often wrong in this respect.

In an attempt to simulate the situation in pyr-FeF$_3$, we have chosen the following exchange model:

$$J_1 = -1 ,$$

$$J_2 = 0 , \qquad (5)$$

$$J_3 = |J_1| / 10 .$$

A model with $J_2 = 0$ and $J_3 \neq 0$ may seem unphysical, however, the second- and third-neighbor bond distances only differ by about 10%. Also, superexchange interactions in insulators are strongly dependent on bond angle and not just bond distance.[22] In addition to this, most models with $J_2 \neq 0$ and $J_3 > 0$ will also stabilize the q=0 phase, as can be seen in Fig. 3. If one believes in universality, then the precise values of J_2 and J_3 are irrelevant as long as the q=0 ordered state is selected. Therefore, we chose to exclude J_2 in order to save computer time. Another model with $J_2 < 0$ and $J_3 = 0$ may also seem tenable. However, Fig. 3 shows that such an exchange model lies precisely on the mean-field phase boundary between a q=0 phase and an incommensurate

phase. The critical properties will almost certainly be affected and complicated by this coexistence, which is undesirable in any preliminary investigation such as this one.

The exchange model in (5) can be pictured if one thinks of the corner-sharing tetrahedral lattice as four interpenetrating fcc lattices. The coupling between the fcc lattices is $J_1 < 0$ and the coupling within each fcc lattice is J_3. Thus, one can think of this model as four ferromagnetic fcc lattices which are mutually intercoupled by strong antiferromagnetic interactions.

Another important question is anisotropy. Fe^{3+} is a spin-$\frac{5}{2}$ ion with a totally symmetric ^6A (S state) ground state. The crystal field around the Fe atoms is very close to perfectly octahedral and the site symmetry is $\overline{3}m$, with the threefold axes along the cubic $\langle 111 \rangle$ directions. Any anisotropy in this system can only arise from mixing of higher level with different spin quantum numbers and is expected to be weak compared to $T_c = 15.4$ K. The anisotropy will be discussed further in Sec. VII.

IV. MONTE CARLO SIMULATIONS

The simulations were carried out using the standard Metropolis spin-flipping algorithm with seven lattice sizes $L \times L \times L$ ($L = 3,4,5,6,7,8,10$). It is important to note that there are 16 spins per unit cell, such that we have 128 spins for $L = 3$ and 16000 spins for $L = 10$. Periodic boundary conditions were implemented in order to eliminate surface effects. Simulation lengths of 50000–200000 Monte Carlo Steps (MCS) per spin were carried out over a wide range of temperatures $0.1 \leq T/|J_1| \leq 1.0$ for $L = 3$. Larger lattices were simulated only in the critical region. For each simulation, 10000–20000 initial MCS were discarded in order to reach equilibrium. The random-spin moves ΔS were attenuated by a factor δ which was adjusted in such a way that roughly 50% of the attempted spin moves were accepted. This increases the efficiency at low temperatures. When a spin move was rejected, the spin was then randomly pivoted around its local exchange field.[23] Such pivoting has no effect on the internal energy but does increase the rate at which phase space is sampled.

All thermodynamic functions were calculated using Ferrenberg and Swendsen's histogram method.[24] The method allows efficient storage and usage of the MC data and most notably the method allows one to calculate all thermodynamic properties as continuous functions of temperature. This feature is extremely useful for locating maxima, minima, and inflection points of thermodynamic quantities, thereby enabling one to obtain accurate estimates of critical temperatures.

The central idea behind the histogram method is to build up information on the energy probability distribution $P_\beta(E)$, where $\beta = 1/T$ is inverse temperature (in units with $k_B = 1$). To be more specific, one calculates a histogram $H_\beta(E)$ which is the number of spin configurations generated between E and $E + \Delta E$. $P_\beta(E)$ is now defined as

$$P_\beta(E_\nu) = \frac{H_\beta(E_\nu)}{Z_\beta} , \qquad (6)$$

$$Z_\beta = \sum_\nu H_\beta(E_\nu) . \qquad (7)$$

Through a simple transformation,[24] one can, in principle, also calculate the probability distribution at any temperature β':

$$P_{\beta'}(E_\nu) = \frac{P_\beta(E_\nu)\exp[(\beta-\beta')E_\nu]}{\sum_\mu P_\beta(E_\mu)\exp[(\beta-\beta')E_\mu]} . \qquad (8)$$

In practice, $P_\beta(E)$ only provides information on the distributions at nearby temperatures since counting statistics in the wings of the distribution $H_\beta(E)$ far from $\langle E \rangle_\beta$ (the average energy) will be poor.

In order to alleviate this problem Ferrenberg and Swendsen have proposed the "multihistogram method," which is an optimized method of combining histogram data for different temperatures and has been implemented in our calculations. For each lattice size at least seven histograms for different temperatures near T_c were combined. In order to follow with temperature quantities like the sublattice magnetization m_s, one must store two-dimensional histograms in the form $H_{\beta,h}(E,m_s)$, where $h = H/T$ is the applied (staggered) field that couples to m_s. Storing two-dimensional histograms is quite costly and can be circumvented if one is only interested in calculating the thermodynamic quantities at one value of the applied field. The idea is to store a one-dimensional histogram $H_\beta(E)$ along with $\langle m_s(E) \rangle_\beta$, $\langle [m_s(E)]^2 \rangle_\beta$, and any other desired moments of m_s.[25] We have stored the first, second, and fourth moments of m_s, which allows calculation of $\langle m_s \rangle, \chi_s$ and the fourth cumulant of m_s (to be discussed later).

Each histogram contained 1000 bins spread over a narrow energy range that the system samples near T_c, instead of the whole energy range from $E/|J_1| = -1.6$ to 0. The actual energy ranges were determined from short trial simulations and varied with lattice size. The important parameter is not the energy range but the bin size ΔE, which varied from $\Delta E/|J_1| = 7.8 \times 10^{-4}$ for $L = 3$ down to $\Delta E/|J_1| = 1.9 \times 10^{-4}$ for $L = 10$. As a check, two histograms with 5000 bins were calculated at T_c for $L = 8$ and 10 and gave virtually identical results.

The model Hamiltonian for the simulations was

$$\mathcal{H} = -\frac{1}{2}J_1 \sum_{\langle ij \rangle_1} \mathbf{S}_i \cdot \mathbf{S}_j - \frac{1}{2}J_3 \sum_{\langle ij \rangle_3} \mathbf{S}_i \cdot \mathbf{S}_j , \qquad (9)$$

where $\langle ij \rangle_1$ and $\langle ij \rangle_3$ represent first- and third-neighbor bonds, respectively, $\mathbf{S}_i = (S_i^x, S_i^y, S_i^z)$ is a unit, three vector on lattice site i, and the exchange constants are described in Eq. (5). The order parameter for the transition is the mean-square sublattice magnetization

$$m_s^2 = \frac{1}{4} \left\langle \sum_{a=1}^4 m_a^2 \right\rangle , \qquad (10)$$

where

$$\mathbf{m}_a = \frac{1}{N} \sum_{i \in a} \mathbf{S}_i \ , \tag{11}$$

where i labels a lattice site, a labels a sublattice within the unit cell, and N is the number of primitive unit cells. The order parameter is also a measure of the normal modes (3):

$$m_s^2 \propto \varphi_1^2 + \varphi_2^2 + \varphi_3^2 \ , \tag{12}$$

because $\mathbf{m}_1 + \mathbf{m}_2 + \mathbf{m}_3 + \mathbf{m}_4 = 0$ in an antiferromagnet. Since the three normal modes φ are three vectors, the full order parameter has nine components. Imposing orthogonality conditions (4) still leaves five continuous rotational degrees of freedom, which is similar to the situation in fcc antiferromagnets.[26] Three of these degrees of freedom are due to Heisenberg symmetry, the remaining two are associated with the arbitrary choice of the relative magnitudes of φ_1, φ_2, and φ_3.

The temperature dependence of the internal energy and heat capacity are shown in Fig. 4. The energy approaches $-1.6|J_1|$ as $T \to 0$, which is in agreement with a simple ground-state calculation. Clear evidence for a phase transition can be seen in the heat capacity near $T/|J_1| = 0.525$. The mean-field transition temperature for this model is

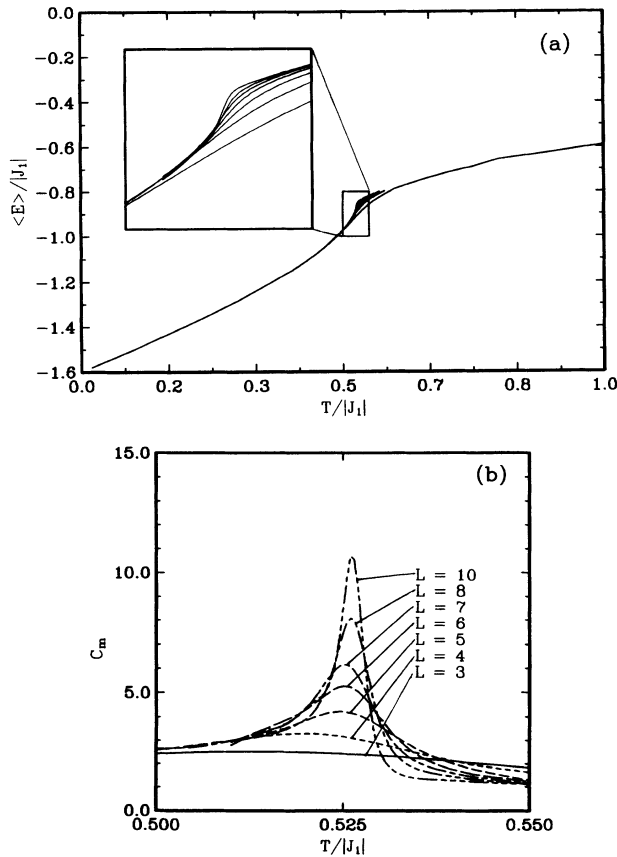$$T_c^{\mathrm{mf}}/|J_1| = \tfrac{1}{3}(2 + 12 J_3/|J_1|) = 1.066\,66 \ .$$

FIG. 4. (a) Internal energy and (b) the heat capacity per spin, for the pyrochlore antiferromagnet with third-neighbor interaction.

The mean sublattice magnetization, m_s, and its corresponding susceptibility,

$$\chi_s = N \frac{|J_1|}{T} (\langle m_s^2 \rangle - \langle m_s \rangle^2) \ , \tag{13}$$

are shown in Fig. 5. The fact that χ_s is diverging strongly at T_c indicates that m_s is the correct order parameter for this transition. At this point it is crucial to determine whether this transition is first order or continuous (critical). This will be discussed in the next section.

V. ORDER OF THE TRANSITION

For the problem at hand, the large number of order-parameter components suggests that the phase transition may be first order. Azaria et al. have conjectured that, for frustrated systems such as the triangular-lattice antiferromagnets, the transitions may indeed be first order. For these reasons we feel it is important to check in great detail for first-order behavior in the pyrochlore system.

One of the central problems in Monte Carlo data studies of phase transitions is determining the order of the transition. Strong first-order transitions will show
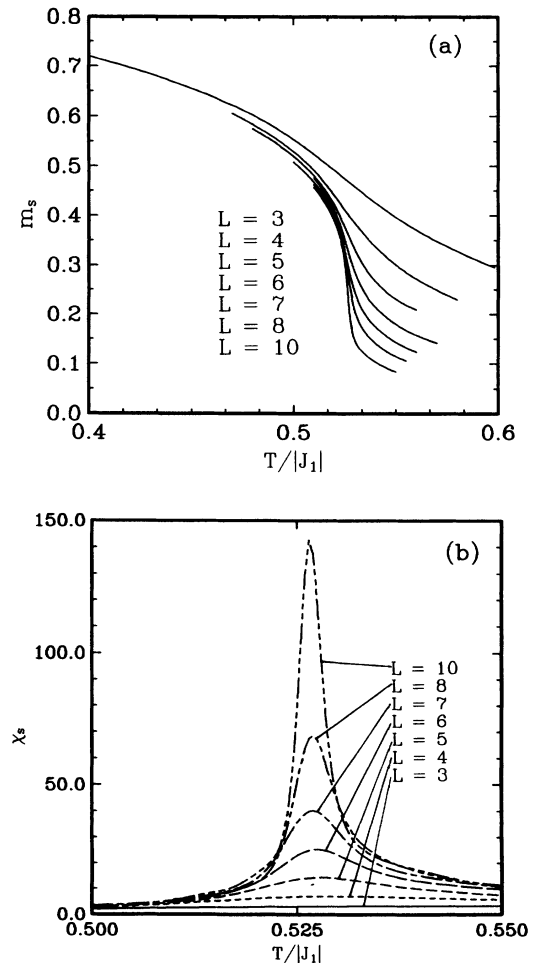

FIG. 5. (a) The mean sublattice magnetization and (b) susceptibility per spin, for the pyrochlore antiferromagnet.

marked discontinuities in thermodynamic quantities such as internal energy and magnetization and present no real problems. Weakly first-order transitions are much more difficult to recognize. This can be understood if one pictures a correlation length ζ, growing as T approaches some virtual critical point, but before that virtual point is reached, the system abruptly changes to the other phase. The correlation length ζ only reaches a critical but finite value, ζ_c. While $\zeta < \zeta_c$, the system will appear to be in the critical region of a continuous transition. It is easy to see that this creates problems if $L < \zeta_c$, where L is the linear extent of the lattice size simulated. Thus, it can always be claimed that any transition that appears to be critical based on MC data is actually weakly first order with $\zeta_c \gg L_{max}$.

Recently there have been significant advances in overcoming this problem. Below we list a number of techniques for detecting a first-order transition.

(1) Discontinuities in the internal energy and magnetization.

(2) Hysteresis in the internal energy and magnetization.

(3) Double peaks in the probability distributions $P(E)$ and $P(m)$.

(4) The heat-capacity and susceptibility maxima should diverge like L^d, where d is the lattice dimensionality.

(5) Half-widths of the heat-capacity and susceptibility peaks should decrease like L^{-d}.

(6) Binders fourth energy cumulant

$$V_L = 1 - \frac{\langle E^4 \rangle}{3 \langle E^2 \rangle} \tag{14}$$

at T_c should approach $\frac{2}{3}$ for a continuous transition and approach some nontrivial value $V^* < \frac{2}{3}$ at a first-order transition.[27]

Methods (1), (2), and (3) are, in fact, three aspects of the same thing and are also rather unreliable for two reasons. For one, if the free-energy barrier which is responsible for the hysteresis is small enough, the MC simulation will sample both phases within the time scale of the simulation, then no hysteresis will be observed. The second and more important reason is that double peaks in the probability distribution have also been observed near continuous transitions in finite systems,[28] as will be discussed further below. The explanation of this is currently unknown. Methods (4) and (5) are also aspects of the same thing. At a first-order transition, the heat-capacity peak is expected to be a δ function which depends on system volume and thus diverges like L^d and narrows like L^{-d}.[29] Both of these ideas are combined in the scaling form of the heat capacity suggested by Challa et al.[27] where one plots $C(T)L^{-d}$ vs $[T - T_c(L)]L^d$. For a first-order transition, the data for all L and T should collapse onto a single line. This works to a high degree of precision for the 10-states ($q = 10$) Potts model but the same is not true for $q = 8$.[30] Method (6) tests the Gaussian nature of the probability distribution $P(E)$ at T_c. If $V = \frac{2}{3}$, then $P(E)$ is Gaussian. For a continuous transition, $P(E)$ is expected to be Gaussian at, as well as away from T_c. For a first-order transition, $P(E)$ will not be Gaussian and therefore $V(T_c) = V^* < \frac{2}{3}$. V^* is related

in a rather transparent indirect way to the latent heat.[27,30] In a sense this is similar to method (3), except much more sensitive, in that small splittings in $P(E)$ for the infinite system that do not result in a double peak for small lattices can be detected. In principle, when $L \to \infty$, the double peak will be eventually resolved for a weak first-order transition. Another advantage of this technique is that the minimum of V_L is expected to approach $\frac{2}{3}$ or V^* as a power law in L, thus allowing one to extrapolate to $L = \infty$.[27] Extrapolating the whole distribution $P(E)$ to $L = \infty$ is not so trivial.

A standard testing ground for these techniques is the q-state Potts model on a two-dimensional lattice, for which the exact solution is known.[31] For $q \leq 4$, the transition is continuous; for $q > 4$, the transition is first order. The $q = 5$ phase change is an example of an extremely weak first-order transition with $\zeta_c \approx 2000$ lattice spacings.[32] For $q = 4$ and 5, $P(E)$ shows double peaks and for $q = 3$, 4, and 5, $P(m)$ is double peaked, providing clear evidence that continuous transitions in finite systems will exhibit double peaks.[28] However, by extrapolating $V_L(min)$ to $L = \infty$, one finds that, for $q = 3$ and 4, $V^* = \frac{2}{3}$ (within statistical accuracy) and for $q = 5$, $V^* < \frac{2}{3}$. Thus, in principle, using this method one can discern a first-order transition by simulating lattices with $L \ll \zeta_c$. Lee and Kosterlitz have proposed an alternative method of dealing with double-peaked distributions[30,33] which they apply to systems with scalar order parameters. It is not yet clear how one applies this method to systems with vector or tensor order parameters.

We now proceed to determine the order of the transition in the pyrochlore model using the ideas discussed above. The first point to make is that the distributions $P(E)$ and $P(m_s)$ were not double peaked at T_c thus making the Lee-Kosterlitz method inapplicable to our problem. Without double peaks, one therefore expects no hysteresis or discontinuities and none were observed. This leaves scaling of the heat capacity and susceptibility with lattice size and the determination of V^*, the last being the most reliable method.[28]

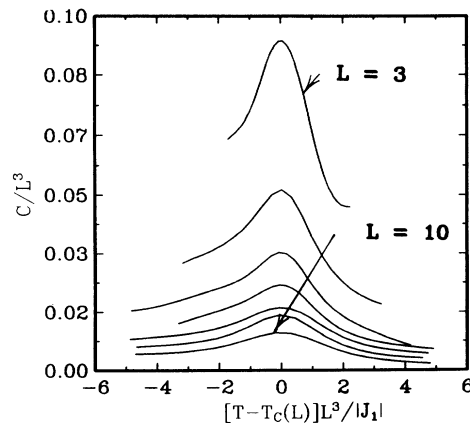Figure 6 shows Challa's heat-capacity scaling plot of

FIG. 6. First-order transition scaling law plot of heat capacity. If the transition is first order, all data should collapse onto a single line, which is not the case.

our data for various lattice sizes. For a first-order transition, the data are expected to collapse onto a single line,[27,30] which is obviously not the case. Figure 7 shows the best fit to C_{max} and χ_{max} as power laws in lattice size. Here we expect

$$C_{max}(L) = C_1 + C_2 L^d ,$$
$$\chi_{max}(L) \propto L^d$$

$$(15)$$

for a first-order transition and

$$C_{max}(L) = C_1 + C_2 L^{\alpha/\nu} ,$$
$$\chi_{max}(L) \propto L^{\gamma/\nu}$$

$$(16)$$

for a continuous transition with periodic boundary conditions. C_1 and C_2 are constants determined in the least-squares-fitting procedure. The best-fit values for the exponents were $\alpha/\nu = 1.7(2)$ and $\gamma/\nu = 3.5(3)$, where the e.s.d.'s were, as usual, determined by a doubling of χ^2 for the fit. The divergence of the heat capacity seems to be significantly weaker than the L^3 behavior expected for a first-order transition. However, the result for the susceptibility is somewhat ambiguous.

In Fig. 8(a) we plot V_L with temperature for all lattice sizes considered. In each case there is a minimum near
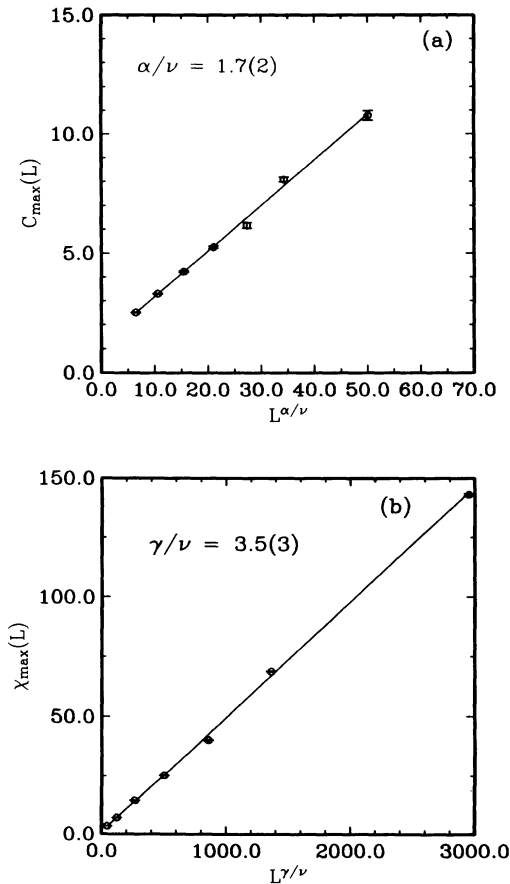
T_c indicating a deviation of $P(E)$ from Gaussian form. Similar to the situation for the heat capacity, $V_{min}(L)$ is also expected to follow a power-law behavior in L,

$$V_{min}(L) = V^* - C_3 L^{-\alpha/\nu} .$$

$$(17)$$

Figure 8(b) shows the best fit to $V_{min}(L)$ giving $V^* = 0.66658(10)$ and $\alpha/\nu = 1.8(2)$ in good agreement with the exponent for C_{max}. V^* is seen to equal $\frac{2}{3}$ to within one e.s.d. In fact, the deviation between V^* and $\frac{2}{3}$ is only 1 part in 10^4. This is more than an order of magnitude closer to $\frac{2}{3}$ than V^* for the 5-state Potts model,[28] which may be the weakest first-order transition known. Considering that this method currently seems to be the best one for determining the order of a phase transition, it is clear we are dealing with a continuous or critical phase transition. At this point we have some information on the critical exponents from C_{max}, χ_{max}, and V_{min}. In the next section we will apply proper finite-size scaling techniques throughout the whole critical region in order to get more information about the exponents.
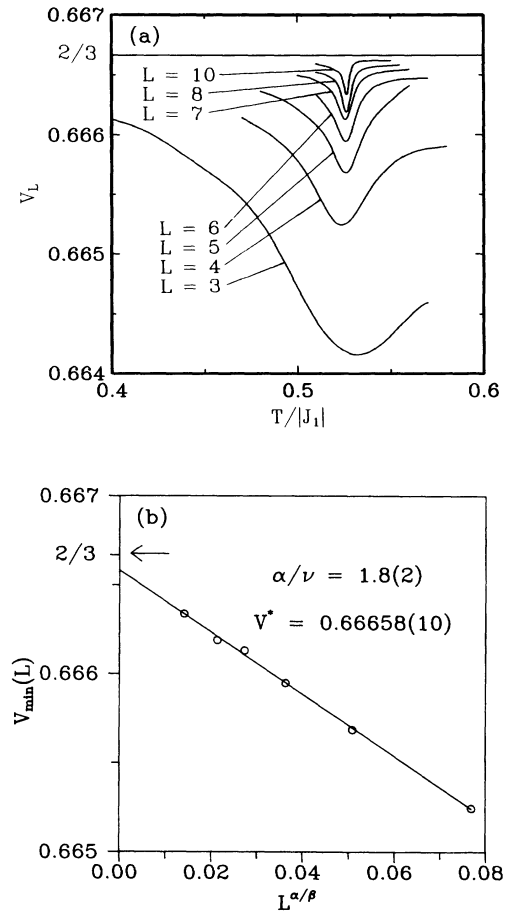

FIG. 7. (a) Dependence of the heat-capacity maximum and (b) the susceptibility maximum, on lattice size. Solid lines represent fits to (16).

FIG. 8. (a) Binder's fourth energy cumulant (see text) near T_c. Deviation of V_L from $\frac{2}{3}$ indicates that $P(E)$ is non-Gaussian. (b) Least-squares fit (solid line) of V_{min} as a power law in lattice size L $(L \geq 4)$, giving $V^* = 0.66658(10)$ and $\alpha/\nu = 1.8(2)$.

VI. CRITICAL EXPONENTS

A well-known fact of finite-size simulations is that the transition temperature tends to shift slightly with changing lattice size. For a critical phase transition one expects[34]

$$T_c(L) = T_c(\infty) + AL^{1/\nu} , \tag{18}$$

where A is a nonuniversal amplitude. Conventionally, $T_c(L)$ is defined by the heat-capacity maximum. However, there are many other methods of defining $T_c(L)$ such as from χ_{max}, V_{min}, and from the inflection point in the magnetization, i.e., the minimum in $m_s' = dm_s/dT$. Other less obvious definitions of T_c have also been proposed[25,35] such as extrema in m'/m, $\langle m^2 \rangle'$, and $\langle m^2 \rangle'/\langle m^2 \rangle$. As it turns out, all of these quantities have different T_c's which may not necessarily be independent. Another quantity which shows an inflection point near $T_c(L)$ is the fourth cumulant of the order parameter[36]

$$U_L = 1 - \frac{\langle m^4 \rangle}{3 \langle m^2 \rangle} . \tag{19}$$

We found that the extrema in U_L' were very strongly dependent on L [i.e., in (18), A was large] which makes extrapolation to $L = \infty$ unreliable. Therefore, these data were not used in the analysis of T_c. It is fairly straightforward to calculate all of these quantities from histogram data and obtain a rather large amount of accurate $T_c(L)$ data. By simultaneously fitting the T_c's from all seven functions described above to the power law (18) (Fig. 9), we obtain $T_c(\infty) = 0.5265(3)$ and $\nu \approx 0.45(5)$. Only lattices with $L \geq 5$ were considered in the fit. The fit was somewhat insensitive to the precise value of ν, however, fixing $\nu = \frac{1}{3} = 1/d$, which would be expected for a first-order transition, gives a decidedly poor fit. It is worth noting that the $T_c(L)$'s approach $T_c(\infty)$ from both above and below, which helps to place a definite window in which $T_c(\infty)$ resides. The unusually accurate value for T_c $(\sigma_{T_c}/T_c \approx 0.0006)$ is a standard feature of the histogram method and is aided by the use of extrema from

seven different thermodynamic functions. Using longer simulations combined with the histogram method, Peczak et al. have managed to obtain an even higher accuracy of $\sigma_{T_c}/T_c \approx 0.0001$ for a Heisenberg ferromagnet.[35]

Next we apply the full finite-size scaling analysis over the whole critical region, following Fisher[34] and Landau.[37] In particular, we will scale m_s, χ_s, and C using the scaling laws

$$m_s(t,L) = L^{-\beta/\nu} f_m(x) , \tag{20a}$$

$$\chi_s(t,L) = L^{\gamma/\nu} f_\chi(x) , \tag{20b}$$

$$C(t,L) = C_{reg}(T) + L^{\alpha/\nu} f_C(x) , \tag{20c}$$

where $x = L^{1/\nu}t$ is the scaling variable, and $C_{reg}(T)$ is the regular or noncritical part of the heat capacity. The scaling functions f are expected to have the following asymptotic behavior:[3,4,37]

$$f_m(x) \propto x^\beta \quad \text{for } T < T_c , \tag{21a}$$

$$f_m(x) \propto x^{\beta - 3\nu/2} \quad \text{for } T > T_c , \tag{21b}$$

$$f_\chi(x) \propto x^{-\gamma} , \tag{21c}$$

$$f_C(x) \propto x^{-\alpha} , \tag{21d}$$

which gives a further check on the exponents.

In Fig. 10 we show $m_s L^{\beta/\nu}$ plotted as a function of the scaling variable $x = L^{1/\nu}t$ using T_c as determined above and $\beta = 0.19$ and $\nu = 0.37$ chosen in such a way that the data for all lattice sizes collapse onto a single line. The slopes at large x give additional exponent estimates, $\beta = 0.17$ and $\beta - 3\nu/2 = -0.35$. In general, it has been found that scaling fluctuation quantities likes C and χ_s is much more difficult than scaling of the order parameter. There are two reasons for this: (1) the statistical error is always larger in fluctuation quantities and (2) the regular part of the heat capacity is unknown and must be accounted for in some empirical manner. In fact, scaling the susceptibility data above T_c was unsuccessful and scaling of the heat capacity was only possible by assuming different regular parts (C^- and C^+) of C above and
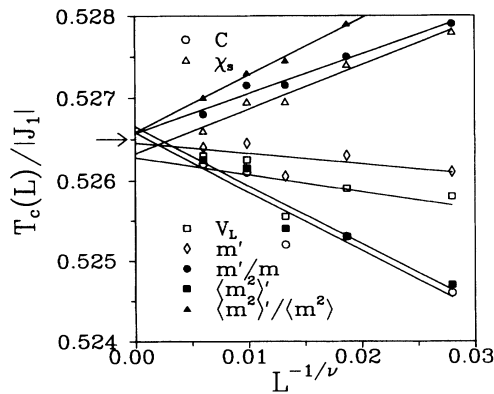

FIG. 9. Scaling of the critical temperatures with lattice size. Solid lines represent fits to (18) giving a mean extrapolated $T_c(\infty) = 0.5265(3)$. The T_c's were obtained from extrema in seven different thermodynamic quantities.
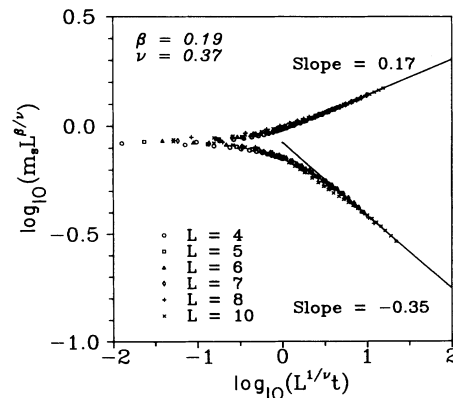

FIG. 10. Finite-size scaling of the order parameter m_s with $\beta = 0.19$ and $\nu = 0.37$ chosen in such a way that all of the data collapse onto a single line. Asymptotic slopes are also shown.
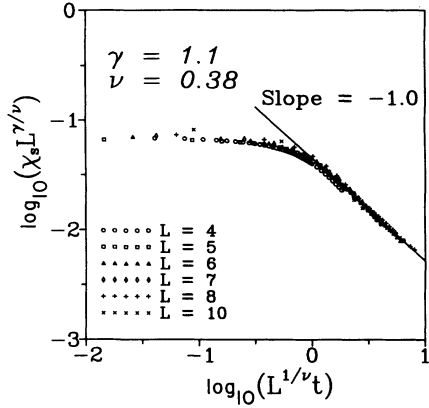
FIG. 11. Same as in Fig. 10 for the staggered susceptibility below T_c, giving $\gamma = 1.1$ and $\nu = 0.38$.

FIG. 13. log-log plot of the sublattice magnetization extrapolated to $L = \infty$ according to (22).

below T_c.[37] The results for scaling χ_s are shown in Fig. 11 giving $\gamma = 1.1$, $\nu = 0.38$, and an asymptotic slope of -1.0. The heat-capacity results (Fig. 12) suffer from statistical noise but scaling is possible if $\alpha = 0.6$ and $\nu = 0.39$. The asymptotic behavior below T_c gives a slope of -0.6 which agrees with (21d), whereas the slope (-1.1) above T_c is far to steep. A possible explanation for this is that some temperature dependence of $C_{reg}(T)$ must be taken into account below T_c.

Recently, Kawamura has suggested a method of extrapolating the magnetization from finite L to $L = \infty$,

$$m_s(L) = m_s(\infty) + \frac{c(T)}{L} , \qquad (22)$$

where the second term arises from spin-wave contributions.[4] As usual, this is only valid for large L. Away from T_c (22) works quite well, however, as one approaches T_c, it necessary to strip away data for small L in order to obtain a good fit. Using data for $L \geq 4$ away from T_c and $L \geq 7$ nearer T_c we have extrapolated our m_s data following (22). The result is shown in Fig. 13 as a function of reduced temperature, with $T_c = 0.5265$. The slope of the line gives $\beta = 0.19(1)$ in good agreement with

all previous results. The e.s.d. in β is most likely underestimated by the fitting procedure since the choice of suitable lattice sizes in (22) was to some degree arbitrary.

At this point we write down estimates of the exponents for this transition in Table I along with the critical exponents for the other two Heisenberg spin universality classes. It is clear that the pyrochlore transition belongs to a new universality class. Again, this does not come as a complete surprise in light of the now well-established results for the TLAF systems. It is well known that critical exponents must obey certain inequalities based on rigorous thermodynamic arguments. The most famous example being the Rushbrooke inequality[38]

$$\alpha + 2\beta + \gamma \geq 2 . \qquad (23)$$

Phenomenological scaling theory[39] predicts that the equality, in fact, holds. Using the pyrochlore exponents in Table I, one finds that $\alpha + 2\beta + \gamma = 2.06(15)$, which satisfies the inequality and agrees with scaling well within statistical error. Another scaling law (actually a hyperscaling law since dimensionality is involved) which lies on less rigorous grounds than (23) is

$$dv + \alpha = 2 . \qquad (24)$$

From Table I we obtain $dv + \alpha = 1.7(1)$, which is not in very good agreement with (24). Fisher has pointed out that this scaling law breaks down in the presence of dangerous irrelevant variables.[40] A resolution of this problem must await a proper renormalization-group treatment.

If the pyrochlore universality class is indeed different, then it is important to determine the symmetry of the order parameter in this system, which is discussed in the next section.
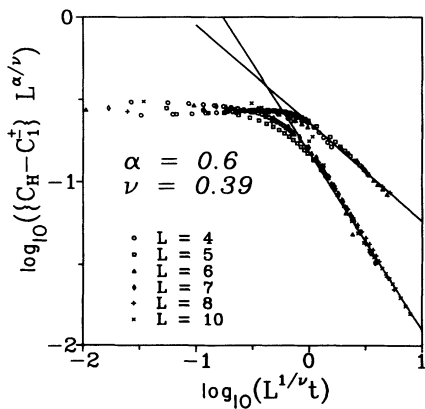

FIG. 12. Same as in Fig. 10 for the heat capacity, giving $\alpha = 0.6$ and $\nu = 0.39$. The regular parts of the heat capacity were chosen as $C^- = 1.1$ and $C^+ = 0.8$.
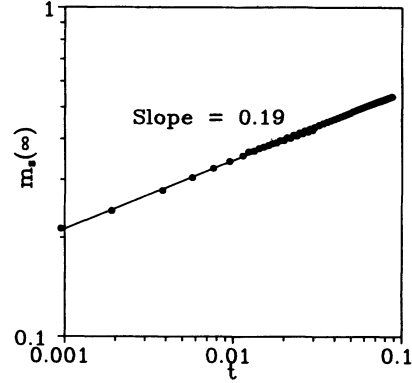
TABLE I. Critical exponents for the three currently known universality classes in Heisenberg spin systems.

	β	γ	ν	α
Pyrochlore	0.18(2)	1.1(1)	0.38(3)	0.6(1)
TLAF (Heis.) (Ref. 4)	0.30(2)	1.17(7)	0.59(2)	0.24(4)
O(3) (Heis.) (Ref. 5)	0.367	1.388	0.707	−0.121

VII. COLLINEARITY

As stated previously, mean-field theory predicted that the relative magnitudes of the three critical models φ_1, φ_2, and φ_3 [see Eq. (3) for a definition] were indeterminate. This results in two extra internal degrees of freedom for the order parameter, over and above the three symmetry degrees of freedom associated with all Heisenberg spin systems. Thus, a collinear structure such as $(\varphi_1 = m_s,\ \varphi_2 = 0,\ \text{and}\ \varphi_3 = 0)$ will be degenerate with noncollinear structures $(\varphi_1 = \varphi_2 = \varphi_3 = m_s/\sqrt{3})$. Figure 14 shows this schematically. Henley has shown by low-temperature expansions that type-I and type-III fcc antiferromagnets prefer collinear ordered states at finite temperature.[26] Thus, thermal fluctuations (beyond the mean-field approximation) will break the internal two-dimensional (2D) degeneracy. In order to check that this is the case in pyrochlores, we have defined and calculated a "collinearity function" for four sublattice antiferromagnets

$$\varphi_{cl} = \frac{3}{2} \frac{\varphi_1^4 + \varphi_2^4 + \varphi_3^4}{(\varphi_1^2 + \varphi_2^2 + \varphi_3^2)^2} - \frac{1}{2} \ . \tag{25}$$

For a collinear structure [Fig. 14(a)] $\varphi_{cl} = 1$ and in the noncollinear limit with spins along the $\langle 111 \rangle$ directions [Fig. 14(b)] $\varphi_{cl} = 0$. The probability distribution $P(\varphi_{cl})$ is shown in Fig. 15 for two lattice sizes at a temperature just below T_c. One can see that the system prefers to be collinear, as conjectured by Henley, with significant fluctuations about the collinear state. The ordered state in pyr-FeF$_3$ is certainly not collinear, therefore there must be a uniaxial anisotropy strong enough to overcome the entropy forces that prefer a collinear state. This immediately raises the question as to whether or not the anisotropy in pyr-FeF$_3$ will affect the critical exponents. A simple answer would be yes. The anisotropy will lower the symmetry of the order parameter and thus change the critical exponents. However, a little more thought reveals that, if the anisotropy is weak, it will only be effective very close to T_c where $|T_c - T|$ is on the order of the anisotropy energy E_{aniso}. Thus, when $|T_c - T| > E_{aniso}$, one will obtain isotropic critical exponents since the system is fluctuating throughout the whole order-parameter space. Crossover to anisotropic exponents will occur at $|T_c - T| \approx E_{aniso}$. A reasonable scenario for FeF$_3$ is that E_{aniso} is on the order of 0.1 K or less and thus beyond the temperature resolution of the experiment. In this case the system modeled in the simulations will
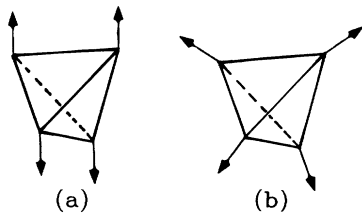

FIG. 14. Examples of (a) collinear and (b) noncollinear spin structures. Thermal fluctuations will select (a) over (b) (Ref. 26).
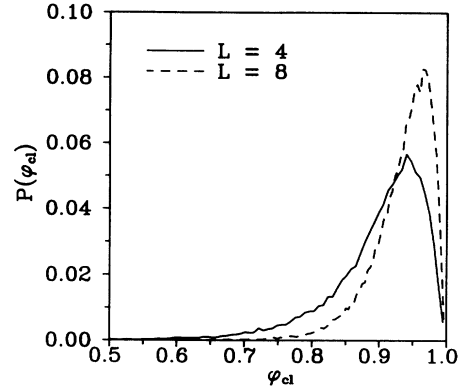

FIG. 15. Probability distribution of the collinearity function φ_{cl} defined in (25), for two different lattice sizes, just below T_c.

reflect the observed behavior in pyr-FeF$_3$. In the presence of the anisotropy, the ordered state is, in fact, twofold degenerate, corresponding to spin arrangements with all spins pointing inwards or outwards on a tetrahedron [Fig. 14(b)]. Naively, one might expect to see 3D Ising critical exponents for such a model, which are certainly not observed in our measurements on pyr-FeF$_3$.

Kawamura has introduced the use of continuous group nomenclature as a means of labeling magnetic order parameters.[3,4,41] This language has long been familiar to gauge theorists. Simple Ising, XY, and Heisenberg order parameters are isomorphic to the groups $\mathbb{Z}_2$, $S_1 = SO(2) = O(2)$, and $S_2 = SO(3)/SO(2)$, respectively. Here it is important not to include redundant symmetries in the group. For example, spatial inversion and rotation about the magnetization axis are redundant symmetry operations for a simple Heisenberg order parameter. The corresponding spaces for the pyrochlore problem are $S_2 \times O(3)$ at the mean-field level, which is reduced to $S_2 \times \mathbb{Z}_3$ for the collinear ordering selected by thermal fluctuations. The S_2 space corresponds to a choice of spin collinearity axis and the $\mathbb{Z}_3$ space maps into the three possible ways of dividing four spins into two pairs.

VIII. SUMMARY AND CONCLUSIONS

pyr-FeF$_3$ exhibits an unusual but highly symmetric, noncoplanar antiferromagnetic order. Neutron-diffraction experiments have been used to follow the sublattice magnetization as a function of temperature, thus allowing the determination of the critical exponent $\beta = 0.18(2)$. This exponent has been verified by Monte Carlo simulations with Heisenberg spins on the same lattice and a suitable exchange model. The phase transition in the simulations is shown to be almost certainly continuous or critical. From the simulations we obtain other exponents $\gamma = 1.1(1)$, $\nu = 0.38(3)$, and $\alpha = 0.6(1)$. These exponents agree well with the Rushbrooke relationship (23), however, hyperscaling does not seem to be as well satisfied. It is clear that these exponents constitute a different universality class. As stated previously, this result is almost to be expected in light of the universality classes predicted and verified in the TLAF's. The simula-

tions also show that a collinear ordered spin arrangement is thermally selected. The agreement between the simulations and experiment is understandable if the anisotropy in FeF_3 that selects the noncollinear state is weak and that the temperatures considered in the experiment are outside the crossover to anisotropic critical properties.

Further work on this problem can proceed along a number of directions. Experimental progress will be dependent on the preparation of better powder samples of pyr-FeF_3 with large particle sizes so that α can be checked with heat-capacity measurements. pyr-FeF_3 is metastable and must be prepared at low temperatures, which means there is little chance of making large single crystals. However, there are may other pyrochlores that have not yet been fully investigated at low temperatures. It is possible that a few will order with the same magnetic structure as in pyr-FeF_3.

There is much theoretical work still to be done on pyrochlores, not only in relation to critical properties but also to understand the spin-glass behavior.[20] A renormalization-group treatment of the problem would almost certainly show many interesting results pertaining to critical properties. Monte Carlo work with anisotropy forces would also be of great interest for two reasons: (1) to determine the strength of the thermal selection and (2) to determine if the critical properties are Ising-like as would be expected from symmetry considerations.

*Present address: Department of Physics, Simon Fraser University, Burnaby, British Columbia, Canada V5A 1S6.

[1] K. Binder and A. P. Young, Rev. Mod. Phys. **58**, 801 (1986).

[2] J. M. Coey, Can. J. Phys. **65**, 1210 (1987).

[3] H. Kawamura, J. Phys. Soc. Jpn. **58**, 584 (1989). The critical exponents quoted are the most up-to-date values available, obtained through private communication with H. Kawamura.

[4] H. Kawamura, J. Phys. Soc. Jpn. **56**, 474 (1987). The critical exponents quoted are the most up-to-date values available, obtained through private communication with H. Kawamura.

[5] M. F. Collins, *Magnetic Critical Scattering* (Oxford University, New York, 1989).

[6] R. B. Griffiths, Phys. Rev. Lett. **24**, 1479 (1970).

[7] H. Kawamura, Phys. Rev. B **38**, 4916 (1988); J. Phys. Soc. Jpn. **59**, 2305 (1990); J. Appl. Phys. **63**, 3086 (1988).

[8] T. E. Mason, M. F. Collins, and B. D. Gaulin, J. Phys. C **20**, L945 (1987); Phys. Rev. B **39**, 586 (1989); H. Kadowaki, S. M. Shapiro, T. Inami, and Y. Ajiro, J. Phys. Soc. Jpn. **57**, 2640 (1988); Y. Ajiro, T. Nakashima, Y. Unno, H. Kadowaki, M. Mekata, and N. Achiwa, *ibid.* **57**, 2648 (1988).

[9] B. D. Gaulin, M. Hagen, and H. R. Child, J. Phys. (Paris) Colloq. **49**, C8-327 (1988).

[10] H. Kadowaki, K. Ubuloski, K. Hirakawa, J. L. Martinez, and G. Shirane, J. Phys. Soc. Jpn. **56**, 1294 (1987).

[11] J. Wang, D. P. Belanger, and B. D. Gaulin, Phys. Rev. Lett. **66**, 3195 (1991).

[12] B. D. Gaulin, T. E. Mason, M. F. Collins, and J. Z. Larese, Phys. Rev. Lett. **62**, 1380 (1989); H. Kawamura, A. Caillé, and M. L. Plumer, Phys. Rev. B **41**, 4416 (1990).

[13] P. Azaria, B. Delamotte, and T. Jolicoeur, Phys. Rev. Lett. **64**, 3175 (1990).

[14] R. De Pape and G. Ferey, Mater. Res. Bull. **21**, 971 (1986).

[15] G. Ferey, R. De Pape, M. Leblanc, and J. Pannetier, Rev. Chem. Min. **23**, 474 (1986).

[16] M. Eibshutz, R. C. Sherwood, F. S. L. Hsu, and D. E. Cox, *Magnetism and Magnetic Materials (Denver, 1972)*, Proceedings of the 18th Annual Conference on Magnetism and Magnetic Materials, AIP Conf. Proc. No. 10, edited by C. D. Graham, Jr. and J. J. Rhyne (AIP, New York, 1973), p. 684.

[17] A. P. Ramirez (unpublished).

[18] A. P. Ramirez, Phys. Rev. B **35**, 5254 (1987).

[19] J. N. Reimers, A. J. Berlinsky, and A.-C. Shi, Phys. Rev. B **43**, 865 (1991).

[20] J. N. Reimers, preceding paper, Phys. Rev. B **45**, 7287 (1992).

[21] J. N. Reimers, J. E. Greedan, R. K. Kremer, E. Gmelin, and M. A. Subramanian, Phys. Rev. B **43**, 3387 (1991); J. E. Greedan, J. N. Reimers, C. V. Stager, and S. L. Penny, *ibid.* **43**, 5682 (1991); J. N. Reimers, J. E. Greedan, S. L. Penny, and C. V. Stager, J. Appl. Phys. **67**, 5967 (1990); J. E. Greedan, M. Sato, X. Yan, and F. S. Razavi, Solid State Commun. **59**, 895 (1986); B. D. Gaulin, J. N. Reimers, J. E. Greedan, T. E. Mason, and Z. Tun (unpublished).

[22] J. B. Goodenough, *Magnetism and the Chemical Bond* (International Publishers, New York, 1963), pp. 165–184.

[23] J. F. Fernandez and T. S J. Streit, Phys. Rev. B **25**, 6910 (1982).

[24] A. M. Ferrenberg and R. H. Swendsen, Phys. Rev. Lett. **61**, 2635 (1988); **63**, 1195 (1988); Comput. Phys. **Sep/Oct**, 101 (1989).

[25] A. M. Ferrenberg (private communication).

[26] C. L. Henley, J. Appl. Phys. **61**, 3962 (1987).

[27] M. S. S. Challa, D. P. Landau, and K. Binder, Phys. Rev. B **34**, 1841 (1986).

[28] M. Fukugita, H. Mino, M. Okawa and A. Ukawa, J. Phys. A **23**, L561 (1990).

[29] Y. Imry, Phys. Rev. B **21**, 2042 (1980).

[30] J. Lee and J. M. Kosterlitz, Phys. Rev. B **43**, 3265 (1991).

[31] For a review see, F. Y. Wu, Rev. Mod. Phys. **54**, 235 (1982); M. N. Barber, in *Phase Transitions and Critical Phenomena*, edited by C. Domb and J. L. Lebowitz (Academic, New York, 1983), Vol. 8.

[32] P. Peczak and D. P. Landau, Phys. Rev. B **39**, 11 932 (1989).

[33] J. Lee and J. M. Kosterlitz, Phys. Rev. Lett. **65**, 137 (1990).

[34] M. E. Fisher, in *Critical Phenomena*, edited by M. S. Green (Academic, New York, 1971); M. E. Fisher and M. N. Barber, Phys. Rev. Lett. **28**, 1516 (1972).

[35] P. Peczak, A. M. Ferrenberg, and D. P. Landau, Phys. Rev. B **43**, 6087 (1991).

[36] K. Binder, Phys. Rev. Lett. **47**, 693 (1981); Z. Phys. B **43**, 119 (1981).

[37] D. P. Landau, Phys. Rev. B **13**, 2997 (1976); **14**, 225 (1976).

[38] G. S. Rushbrooke, J. Chem. Phys. **39**, 842 (1963).

[39] B. Widom, J. Chem. Phys. **43**, 3892 (1965); **43**, 3898 (1965); L. P. Kadanoff, Physics **2**, 263 (1966); L. P. Kadanoff, W. Götze, D. Hamblen, R. Hecht, E. A. Lewis, V. V. Palciauskas, M. Rayl, and J. Swift, Rev. Mod. Phys. **39**, 395 (1967).

[40] M. E. Fisher, in *Critical Phenomena, Proceedings, Stellenbosch, South Africa 1982,* edited by F. J. W. Hahne (Springer, Berlin, 1983).

[41] H. Kawamura, J. Phys. Soc. Jpn. **59**, 2305 (1990).